Electronic Supplementary Material (ESI) for RSC Advances.

Supplementary Information

New Route to Nanoscale Ceramics in Asymmetric Reaction Fields of Carbon Nanospaces

Tomonori Ohba,* Yuki Ohyama, and Hirofumi Kanoh

Graduate School of Science, Chiba University, 1-33 Yayoi, Inage, Chiba 263-8522, Japan

*E-mail: ohba@pchem2.s.chiba-u.ac.jp

Experimental Details

Preparation of $BaTiO_3$. Barium ethoxide (>99%, Kojundo Chemical Laboratory) and titanium tetraisopropoxide (>99%, Kojundo Chemical Laboratory) were used as precursors. Methanol (>99%, Wako Pure Chemical Industries, Ltd.) and methoxyethanol (>99%, Wako Pure Chemical Industries, Ltd.) were used as the solvent. The volume ratio of methanol to methoxyethanol was maintained at 3:2. Barium ethoxide solution was prepared by dissolving barium ethoxide in methanol–methoxyethanol solvent by stirring with a magnetic stirrer for several minutes, in a N_2-filled glove box (300 ppm of O_2 and H_2O). Two solutions of barium ethoxide solution and titanium tetraisopropoxide were subsequently mixed in 2:1 molar ratios (the Ba/Ti molar ratio was 2) and stirred for 3 h at 500 rpm. The concentrations of titanium tetraisopropoxide were 50, 100, 200, 400, and 600 mmol L^{-1}. ACFs (Ad'all W15) were soaked in the mixed solution for confined-$BaTiO_3$ preparation. For nano-$BaTiO_3$ preparation, a mixed solution without impregnated ACFs was used for the subsequent hydrolysis reaction. Hydrolysis was initiated by addition of 5–20 times the volume of water after the two stock solutions were mixed, and stirring in a Teflon-lined stainless-steel autoclave. The solvothermal reaction of the final suspension in the autoclave was conducted at 400 K for 24 h. The resultant product was repeatedly rinsed with boiling water and dried at 333 K. Micro-$BaTiO_3$ and crystalline-$BaTiO_3$ were prepared using barium carbonate (>98%, Wako Pure Chemical Industries, Ltd.) and rutile-type titanium dioxide (>99%, Wako Pure Chemical Industries, Ltd.) A stoichiometric mixture of barium carbonate and titanium dioxide was thoroughly ground, and pressed into a pellet under more than 60 MPa for 30 min. The pellets were heat treated at 1073 K or 1173 K for 24 h for micro-$BaTiO_3$, and 1073 K for 24 h, 1373 K for 24 h, and 1473 K for 48 h for crystalline-$BaTiO_3$, followed by grinding and pelletizing. The scheme of the preparation process is shown in Fig. S1.

Characterization. XRD patterns of $BaTiO_3$ were collected with a Rigaku Ultima IV diffractometer at room temperature, using Cu Kα radiation (λ = 0.1541 nm), at 40 kV and 40 mA. The patterns were collected in step-mode with a resolution of 0.01° and a count time of 3 s for each step from 10 to 90°. Crystallite sizes were evaluated from the Scherrer equation, $D = 0.89\lambda/(B\cos\theta)$, using full-width at half-

maximum values of several selected profiles, where D, B, and θ are the particle size, full-width at half-maximum of a peak, and scattering angle, respectively. The particle sizes were observed using TEM (JEOL JEM-2100F) at 120 kV and SEM (JEOL JSM-6335F) at 2–5 kV. High-angle annular dark-field scanning TEM and electron-dispersion spectroscopy were performed using the JEOL JEM-2100F at 200 kV. Finely ground $BaTiO_3$ crystals were dispersed in ethanol and placed on grids prior to TEM measurements. TG analysis of confined-$BaTiO_3$ was performed, using a Shimadzu DTG-60AH instrument, by heating from room temperature to 1200 K at a rate of 10 K min^{-1} under a dried air flow of 100 mL min^{-1}. The N_2 adsorption isotherms at 77 K were measured using a Quantachrome Autosorb-1 instrument. $BaTiO_3$ crystals were heated at 423 K below 0.1 mPa for more than 2 h prior to measurement of the N_2 adsorption isotherms. Raman spectroscopy of $BaTiO_3$ was performed using a 1 mW Nd:YAG laser (NRS-3100, JASCO Co., Japan).

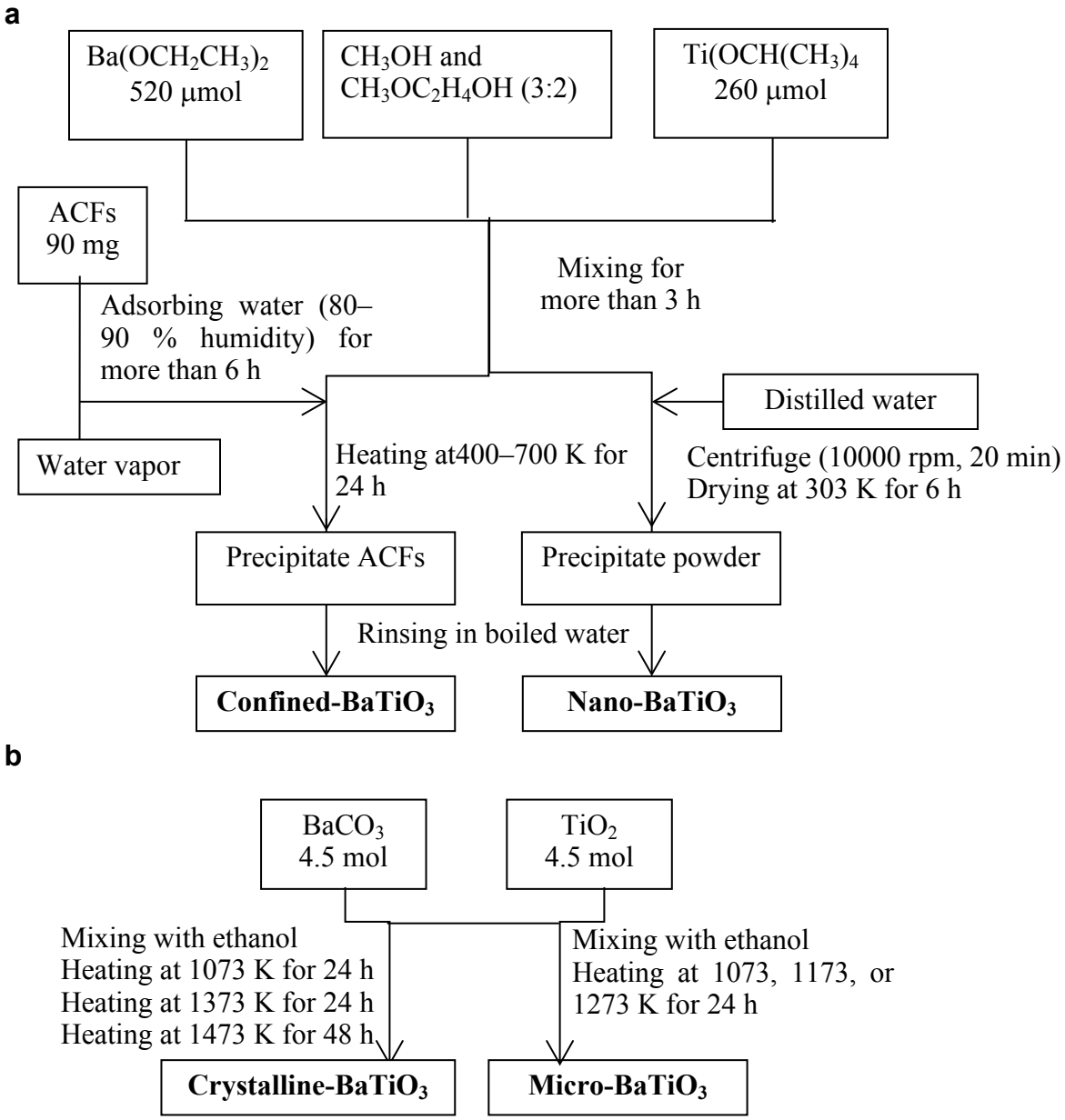

Figure S1. Schematic representation of preparation of $BaTiO_3$ by sol–gel solvothermal (a) and solid-state (b) reactions.

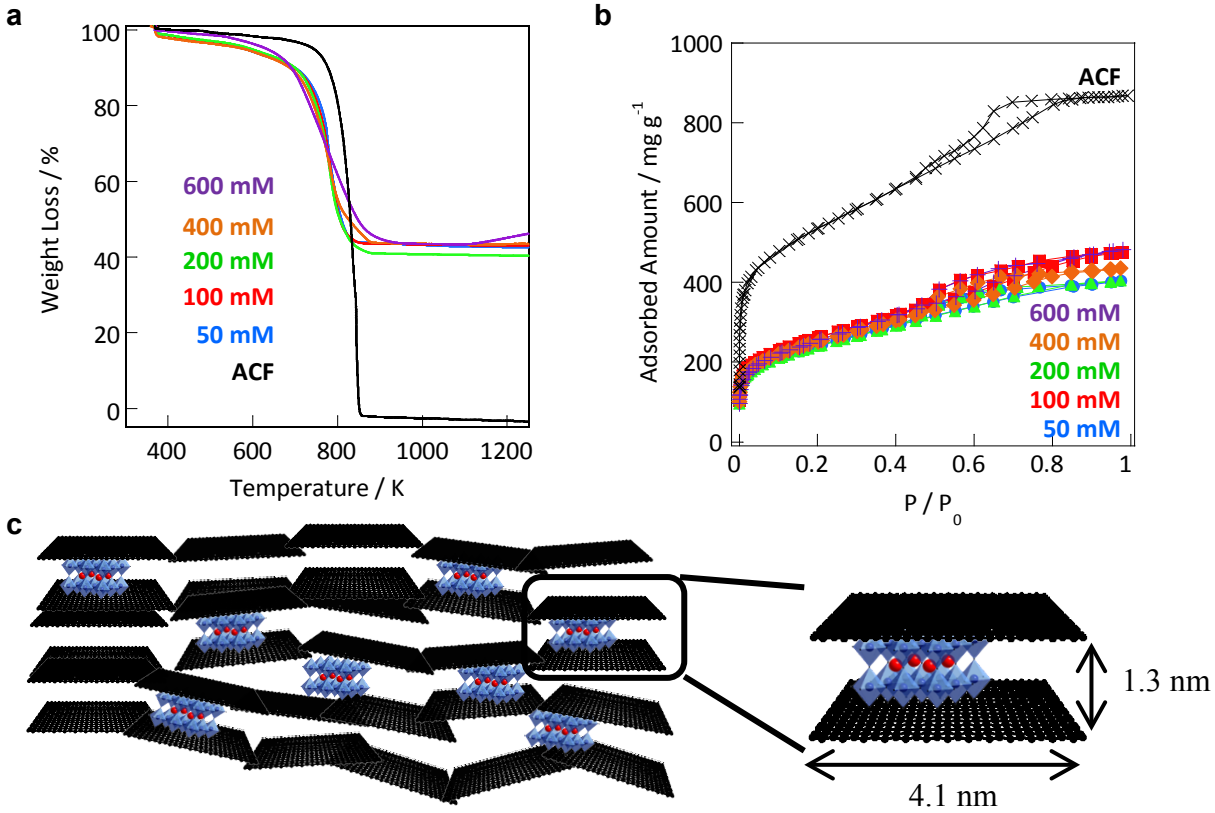

Figure S2. (a) TG measurements of confined-$BaTiO_3$ and ACFs in dried air atmosphere as function of temperature. Weight losses indicate ACF combustion. Amounts of residue after TG measurements were 40–45% for all confined-$BaTiO_3$ samples, but no residue was observed for ACFs, indicating that the weight ratios of $BaTiO_3$ to ACFs were 67–82%. This suggests that ACF nanopore volumes of 0.11–0.14 mL g^{-1} are occupied by $BaTiO_3$ particles, calculated using a $BaTiO_3$ density of 6.02 g mL^{-1}. (b) N_2 adsorption isotherms of confined-$BaTiO_3$ and ACFs at 77 K. The decreases in N_2 adsorbed amounts for confined-$BaTiO_3$ compared with ACFs were attributed to the occupation by $BaTiO_3$ of carbon nanospaces. Nanopore volumes and specific surface areas obtained by α_S analysis of N_2 adsorption isotherms decreased from 1.04 mL g^{-1} to 0.46–0.50 mL g^{-1}, and from 1600 m^2 g^{-1} to 750 m^2 g^{-1}. The significant decreases compared with the estimated occupancies obtained using TG, mentioned above, suggest that confined-$BaTiO_3$ is present in the ACF nanopores, because of significant blocking of N_2 penetration into these nanopores. (c) Schematic image of confined-$BaTiO_3$ in nanopores, based on the above TG results and N_2 adsorption isotherms. The average nanopore width and length were 1.3 and 4 nm, respectively, determined from α_S analysis and (10) peaks in the XRD of ACFs. Red spheres, blue octahedrons, and black rectangles indicate Ba, TiO_3, and ACF carbon walls, respectively.

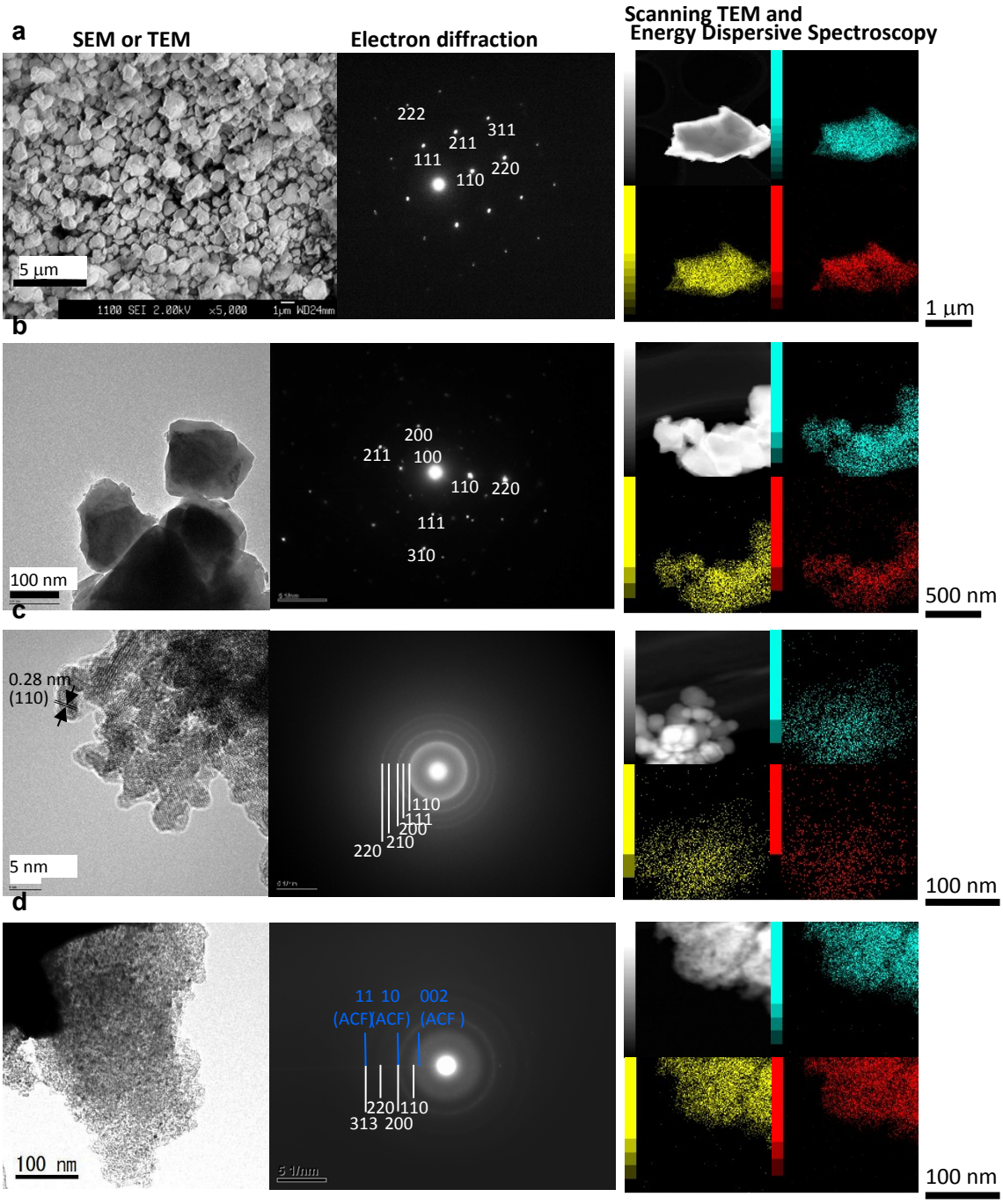

Figure S3. SEM or TEM images, electron diffraction patterns (the same as in Fig. 2), high-angle annular dark-field scanning TEM images, and energy-dispersive spectroscopic images of crystalline-$BaTiO_3$ (a), micro-$BaTiO_3$ (b), nano-$BaTiO_3$ (c), and confined-$BaTiO_3$ (d). The microscopic images show similar particle sizes to those in Fig. 2. Electron diffraction patterns of particles have peaks originating from $BaTiO_3$ crystals, and energy-dispersive spectroscopy suggests that these particles are composed of Ba, Ti, and O atoms, therefore these particles are various types of $BaTiO_3$ crystals.

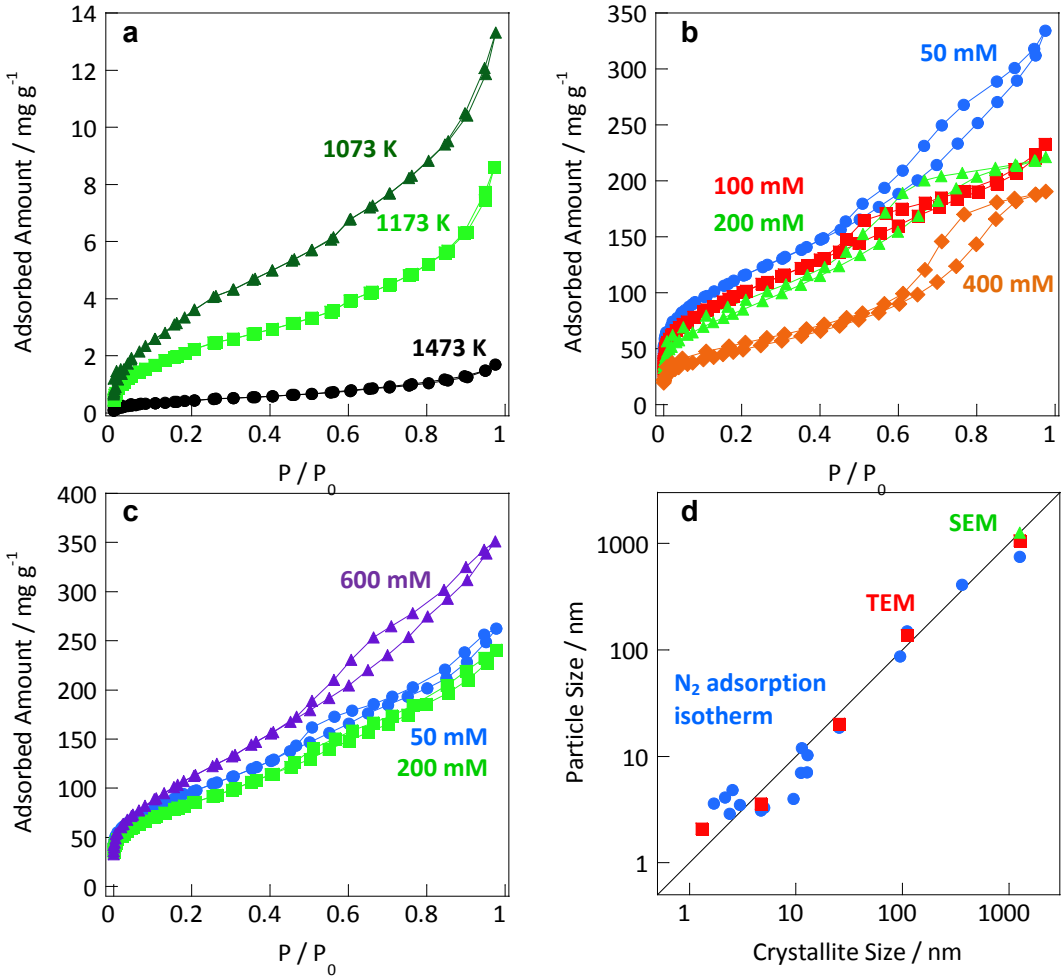

Figure S4. N_2 adsorption isotherms at 77 K for evaluating and comparing $BaTiO_3$ particle sizes. N_2 adsorption isotherms of crystalline- and micro-$BaTiO_3$ (a), nano-$BaTiO_3$ (b), and confined-$BaTiO_3$ after removal of ACFs by combustion at 673 K for 48 h (c). BET specific surface areas of crystalline-$BaTiO_3$, and micro-$BaTiO_3$ at 1273, 1173 and 1073 K were 1.3, 2.4, 6.7, and 11.5 $m^2\ g^{-1}$, respectively, corresponding to particle diameters of 750, 408, 150, and 87 nm, respectively, assuming spherical particles. In the same way, the particle sizes of nano-$BaTiO_3$ were 3.1, 3.5, 4.8, and 7.0 nm for Ti concentrations of 50 (323 $m^2\ g^{-1}$), 100 (285 $m^2\ g^{-1}$), 200 (207 $m^2\ g^{-1}$), and 400 mM (143 $m^2\ g^{-1}$), respectively. The particle sizes of confined-$BaTiO_3$ were 3.6, 4.1, and 2.9 nm for Ti concentrations of 50 (278 $m^2\ g^{-1}$), 200 (246 $m^2\ g^{-1}$), and 600 mM (340 $m^2\ g^{-1}$), respectively. (d) Comparison of particle diameters evaluated from N_2 adsorption isotherms and TEM or SEM images with crystallite sizes evaluated from XRD.

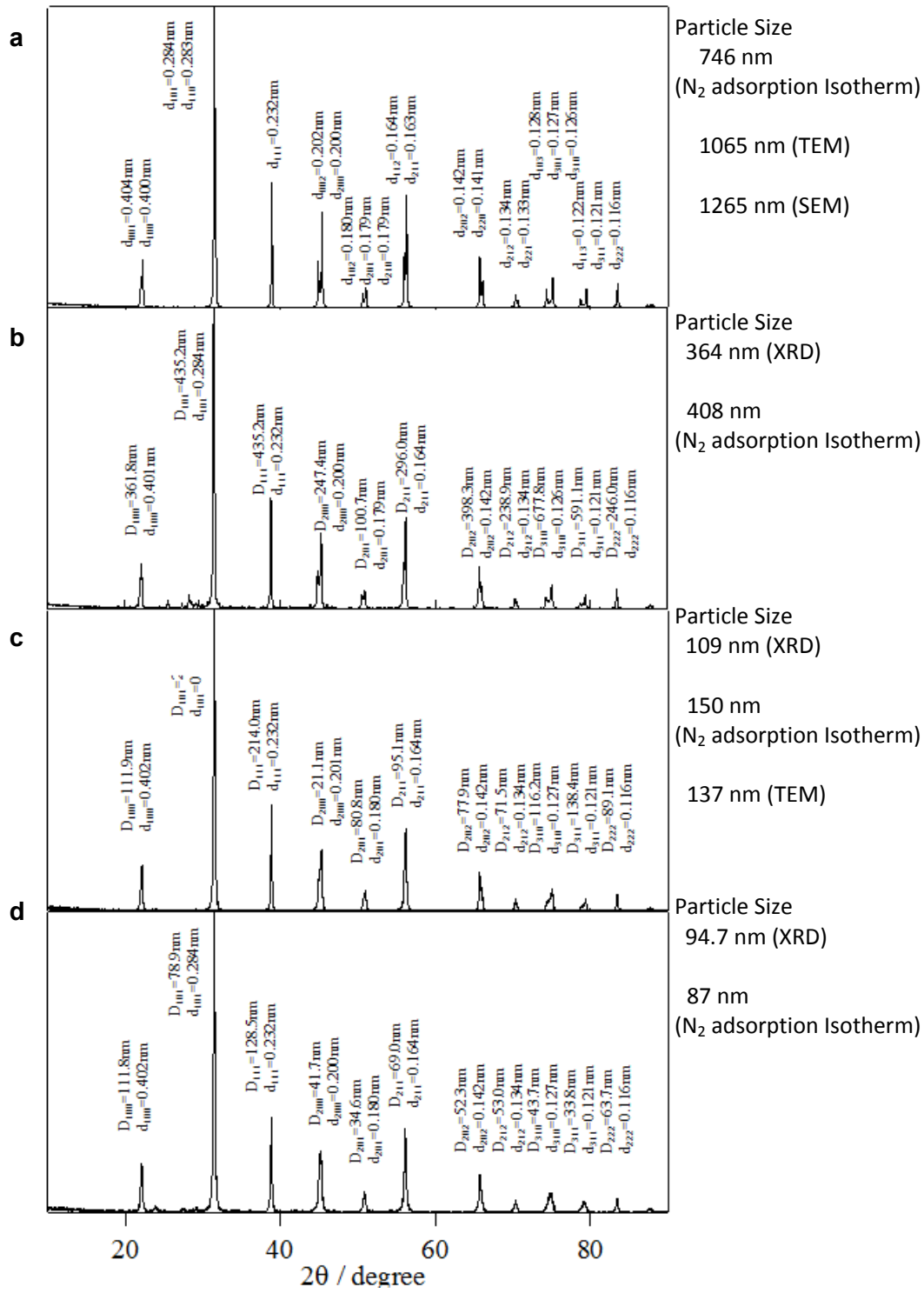

Figure S5-1. Evaluation of $BaTiO_3$ crystal structures. XRD patterns of crystalline-$BaTiO_3$ (a), and micro-$BaTiO_3$ prepared by heat treatment at 1273 K (b), 1173 K (c), and 1073 K, with corresponding particle sizes.

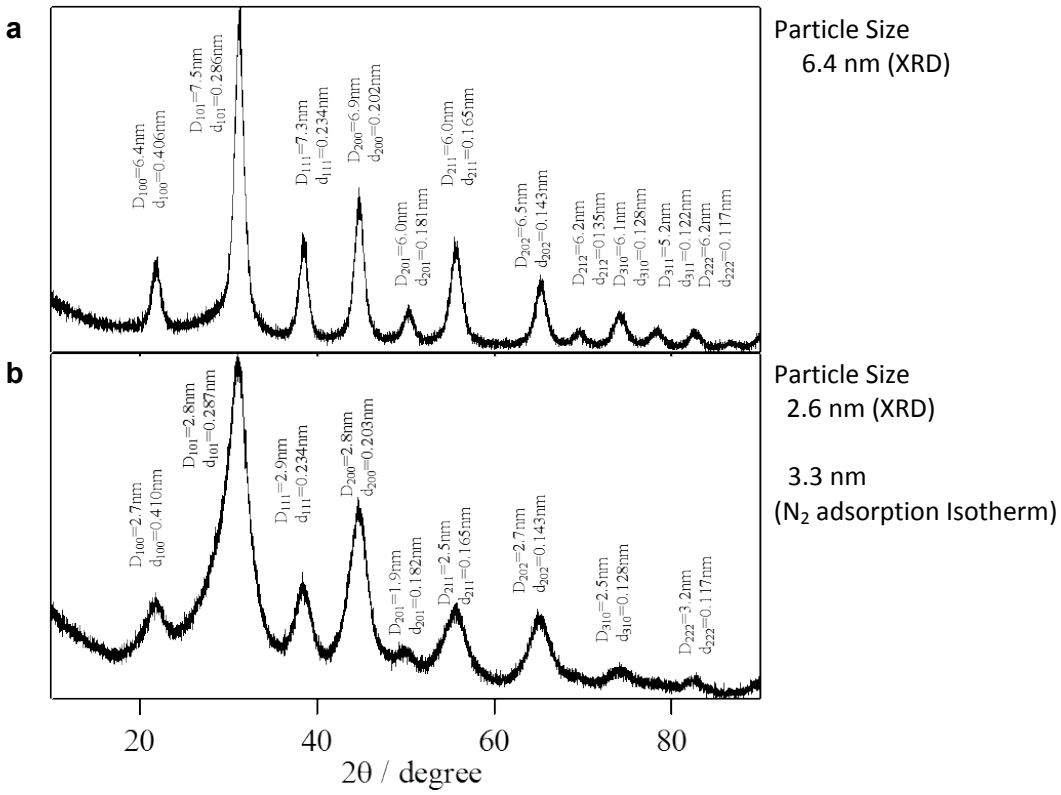

Figure S5-2. Evaluation of $BaTiO_3$ crystal structures. XRD patterns of nano-$BaTiO_3$ prepared under conditions [Ba] = 800 mmol L^{-1}, [Ti] = 400 mmol L^{-1}, and heat treatment at 400 K, with corresponding particle sizes.

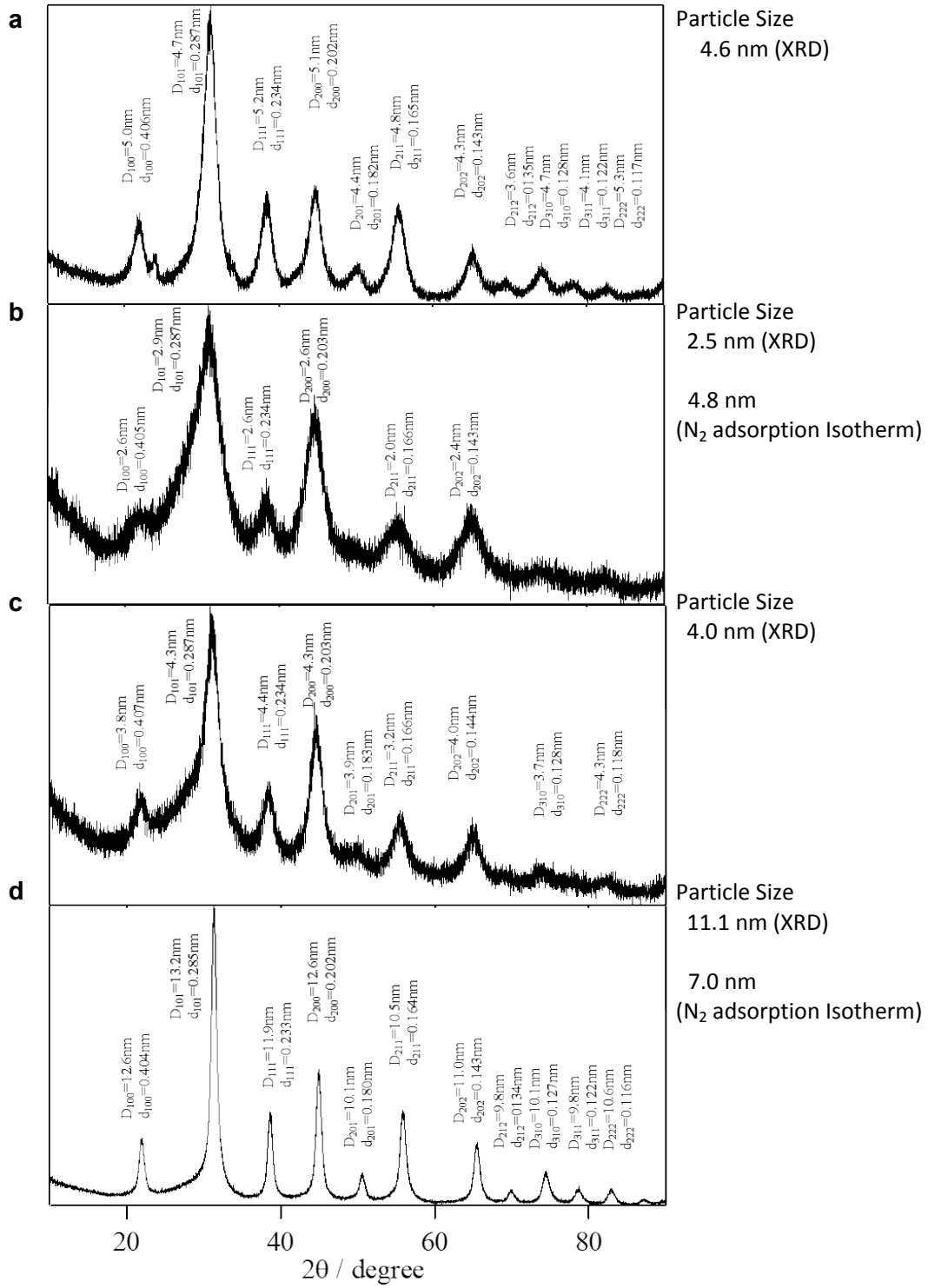

Figure S5-3. Evaluation of $BaTiO_3$ crystal structures. XRD patterns of nano-$BaTiO_3$ prepared under conditions [Ba] = 400 mmol L^{-1} and [Ti] = 200 mmol L^{-1} (a–c), or [Ba] = 400 mmol L^{-1} and [Ti] = 400 mmol L^{-1} (d), and heat treatment at 400 K, with corresponding particle sizes.

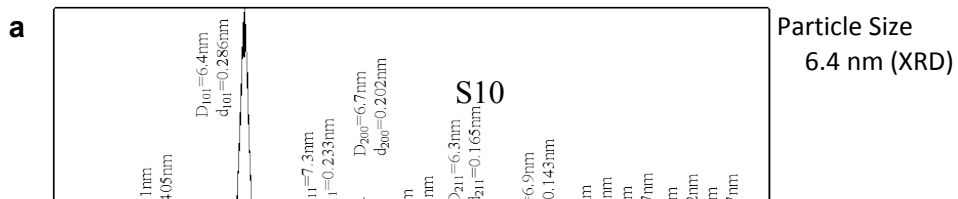

Figure S5-4. Evaluation $BaTiO_3$ crystal structures. XRD patterns of nano-$BaTiO_3$ prepared under conditions [Ba] = 400 mmol L^{-1} and [Ti] = 200 mmol L^{-1}, and heat treatment at 600 K, with corresponding particle sizes.

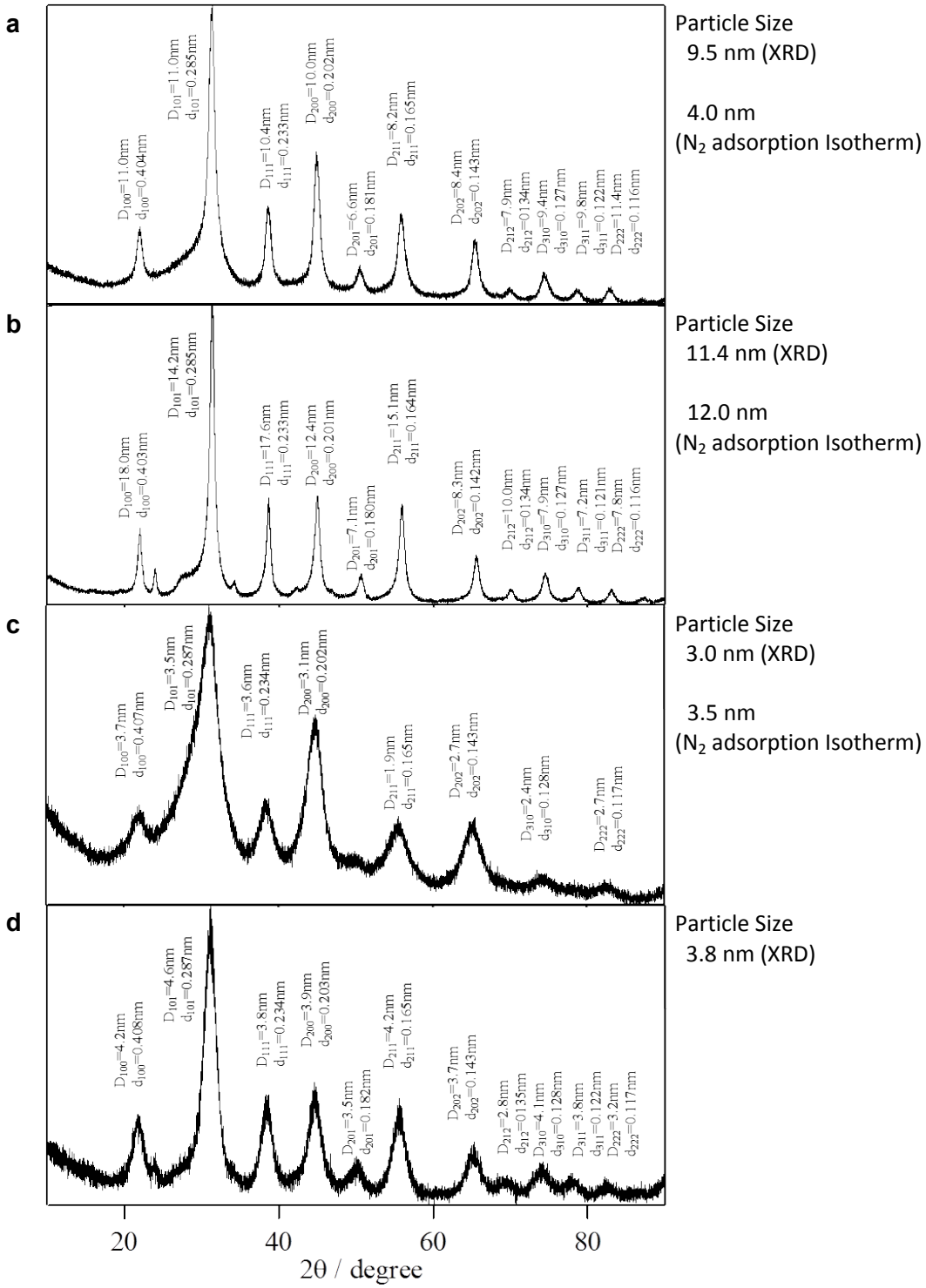

Figure S5-5. Evaluation of $BaTiO_3$ crystal structures. XRD patterns of nano-$BaTiO_3$ prepared under conditions [Ba] = 200 mmol L^{-1} and [Ti] = 200 mmol L^{-1} (a, b), or [Ba] = 200 mmol L^{-1} and [Ti] = 100 mmol L^{-1} (c, d), and heat treatment at 400 K, with corresponding particle sizes.

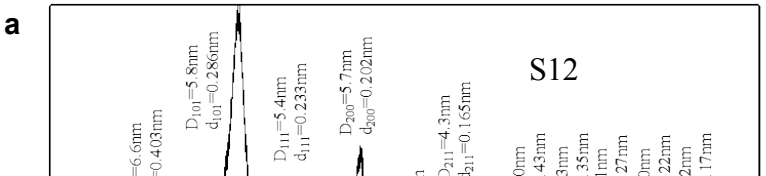

Figure S5-6. Evaluation of $BaTiO_3$ crystal structures. XRD patterns of nano-$BaTiO_3$ prepared under conditions [Ba] = 100 mmol L^{-1} and [Ti] = 50 mmol L^{-1} (a–c), or [Ba] = 100 mmol L^{-1} and [Ti] = 100 mmol L^{-1} (d), and heat treatment at 400 K, with corresponding particle sizes.

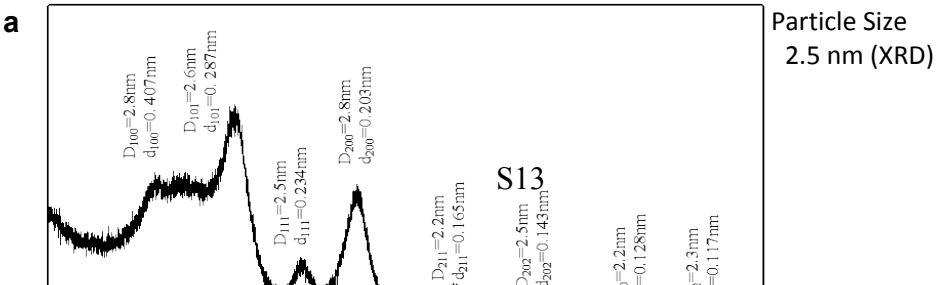

Figure S5-7. Evaluation of $BaTiO_3$ crystal structures. XRD patterns of confined-$BaTiO_3$ prepared under conditions [Ba] = 800 mmol L^{-1} and [Ti] = 400 mmol L^{-1}, and heat treatment at 400 K, with corresponding particle sizes.

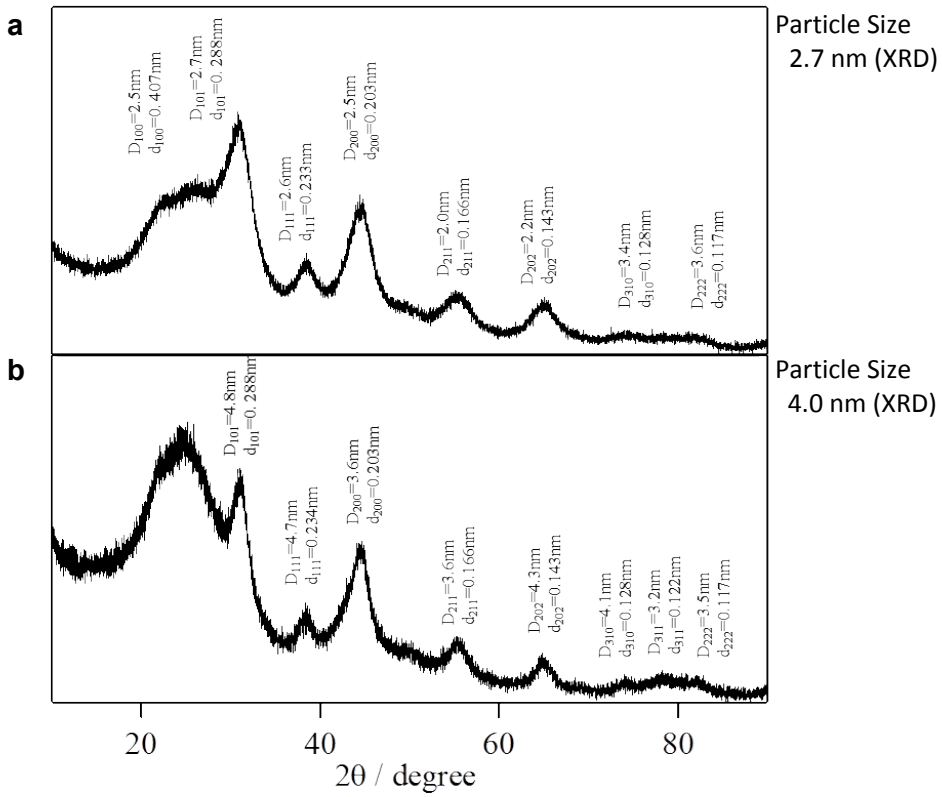

Figure S5-8. Evaluation of $BaTiO_3$ crystal structures. XRD patterns of confined-$BaTiO_3$ prepared under conditions [Ba] = 800 mmol L^{-1} and [Ti] = 400 mmol L^{-1}, and heat treatment at 400 K, with corresponding particle sizes.

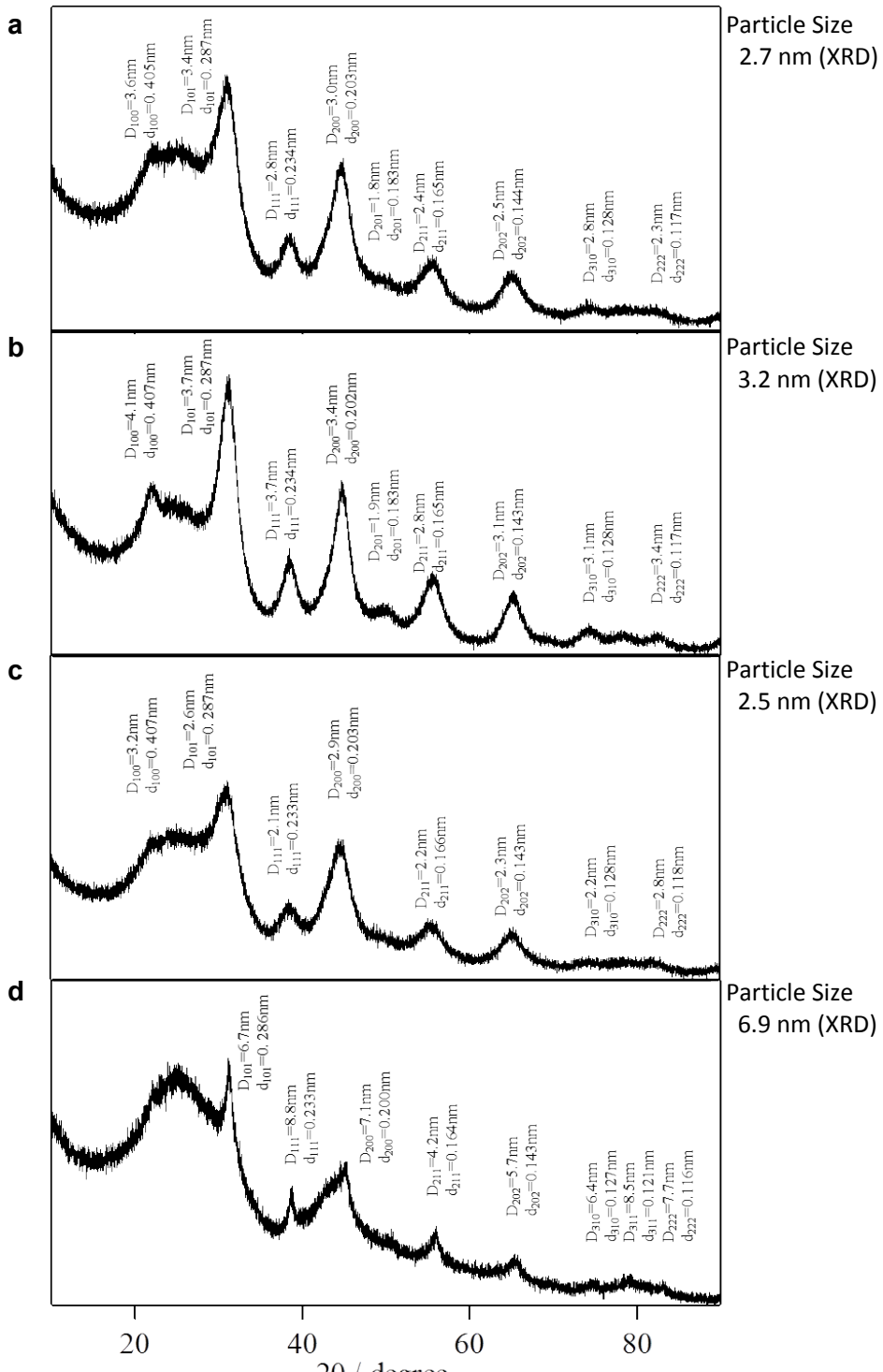

Figure S5-9. Evaluation of $BaTiO_3$ crystal structures. XRD patterns of confined-$BaTiO_3$ prepared under conditions [Ba] = 400 mmol L^{-1} and [Ti] = 200 mmol L^{-1}(a–c), or [Ba] = 400 mmol L^{-1} and [Ti] = 400 mmol L^{-1} (d), and heat treatment at 400 K, with corresponding particle sizes.

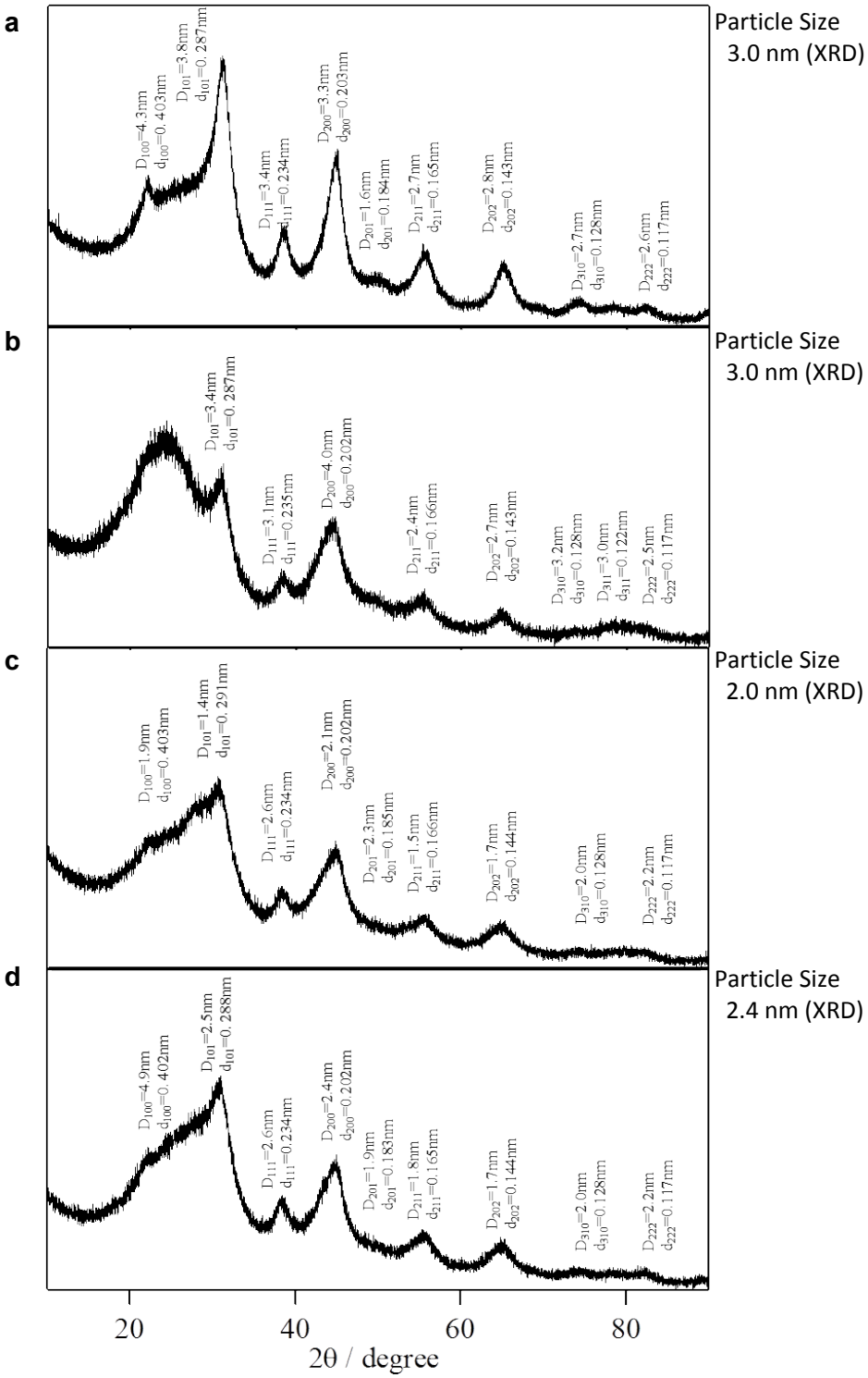

Figure S5-10. Evaluation of $BaTiO_3$ crystal structures. XRD patterns of confined-$BaTiO_3$ prepared under conditions [Ba] = 200 mmol L^{-1} and [Ti] = 100 mmol L^{-1}, and heat treatment at 400 K, with corresponding particle sizes.

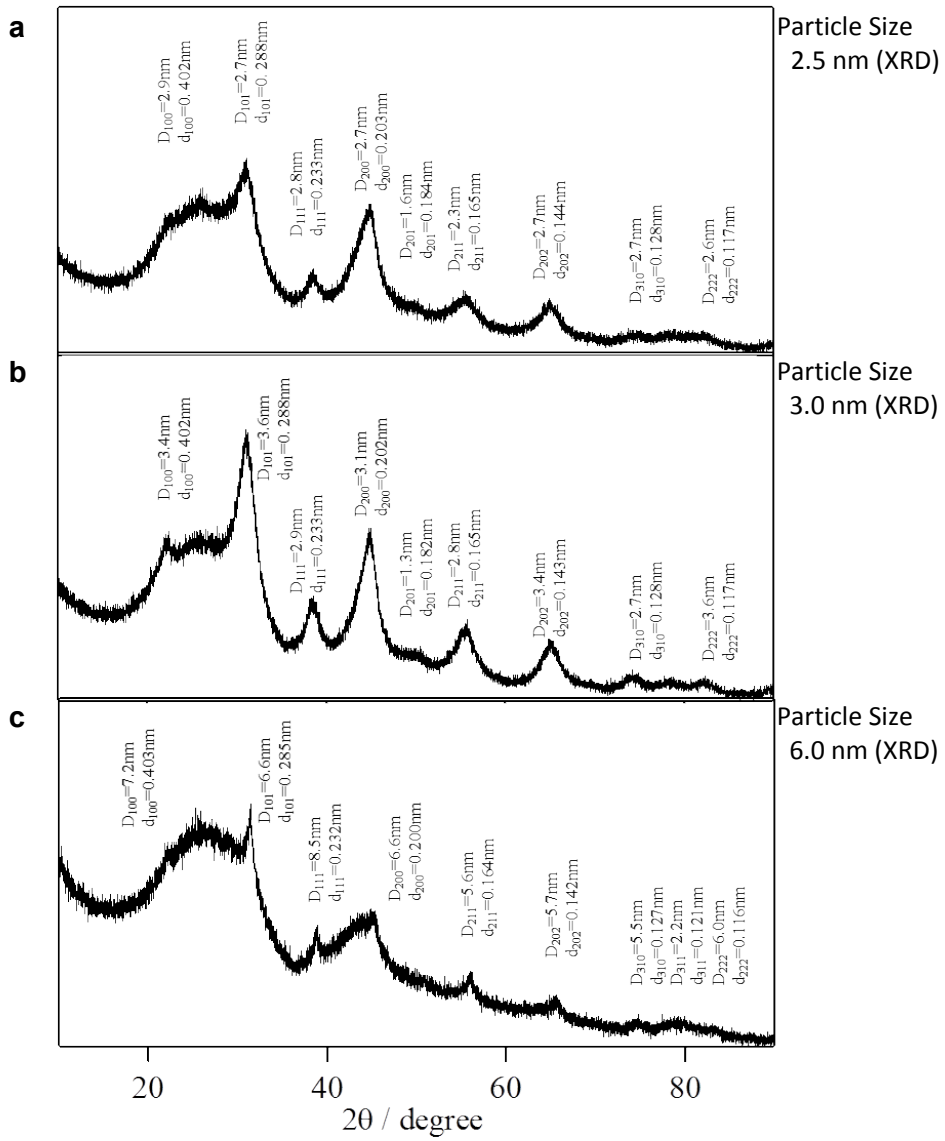

Figure S5-11. Evaluation of $BaTiO_3$ crystal structures. XRD patterns of confined-$BaTiO_3$ prepared under conditions [Ba] = 200 mmol L^{-1} and [Ti] = 100 mmol L^{-1}(a, b), or [Ba] = 200 mmol L^{-1} and [Ti] = 200 mmol L^{-1} (c), and heat treatment at 400 K, with corresponding particle sizes.

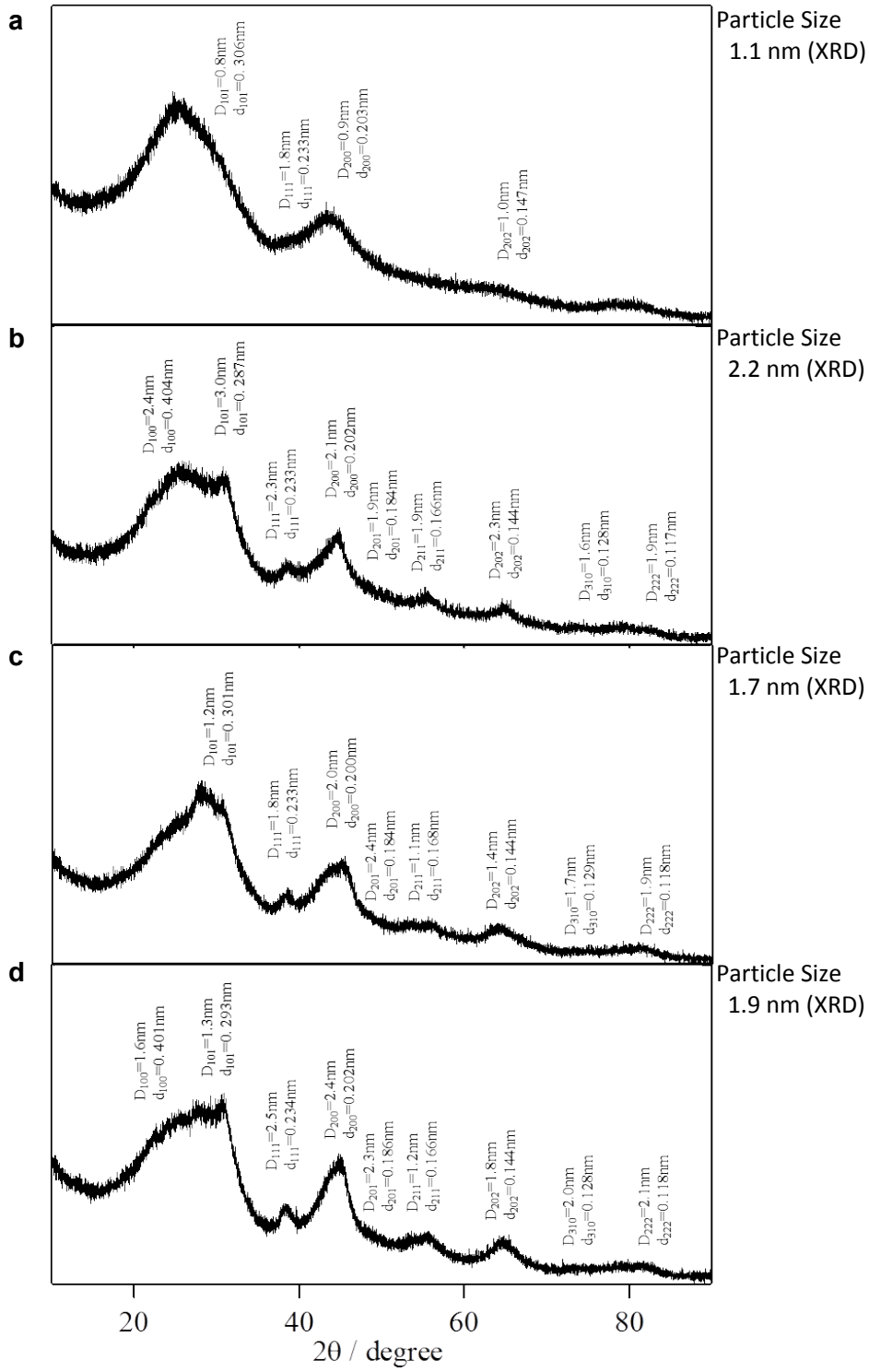

Figure S5-12. Evaluation of $BaTiO_3$ crystal structures. XRD patterns of confined-$BaTiO_3$ prepared under conditions [Ba] = 100 mmol L^{-1} and [Ti] = 50 mmol L^{-1}, and heat treatment at 400 K, with corresponding particle sizes.

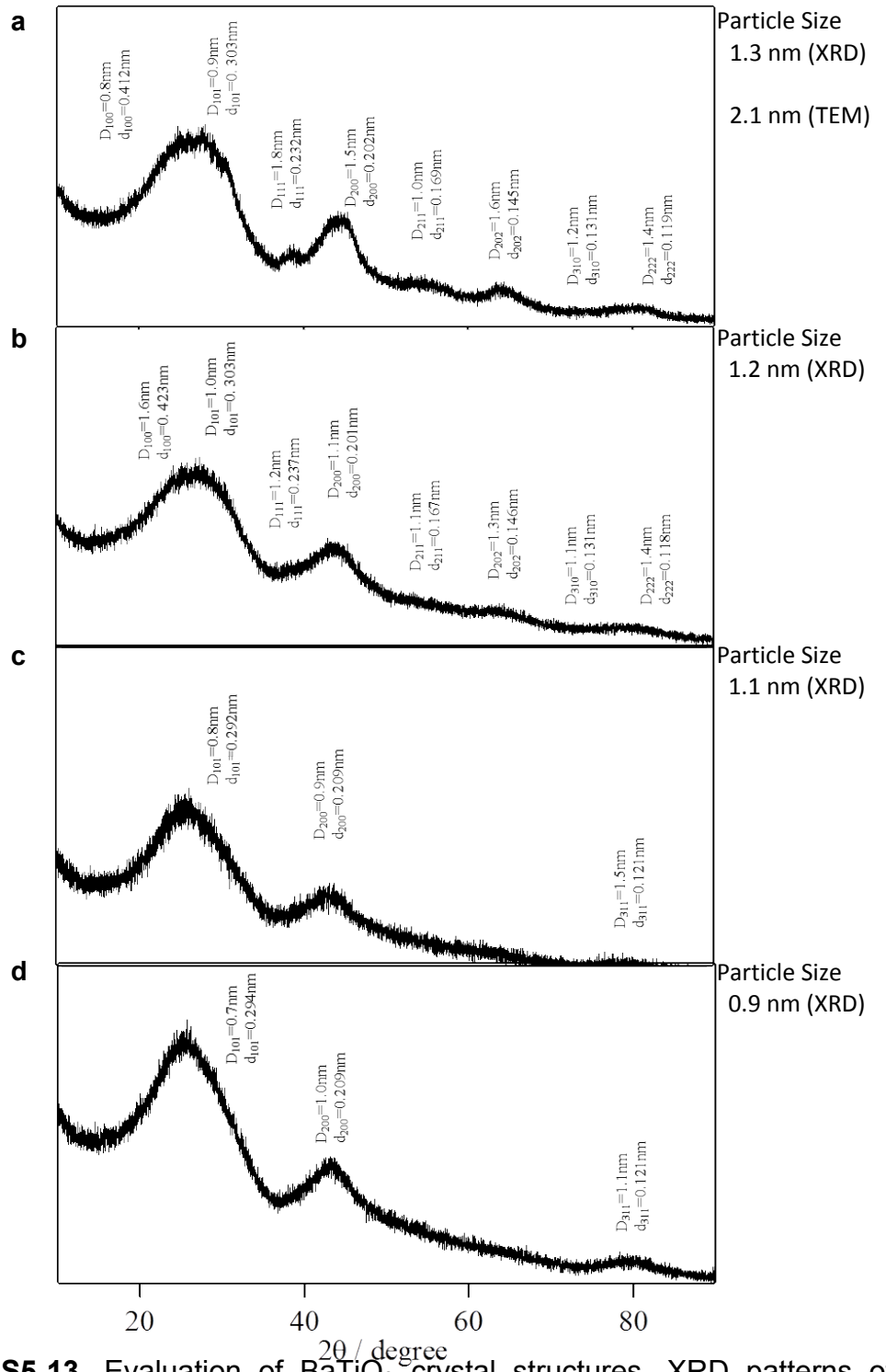

Figure S5-13. Evaluation of $BaTiO_3$ crystal structures. XRD patterns of confined-$BaTiO_3$ prepared under conditions [Ba] = 100 mmol L^{-1} and [Ti] = 50 mmol L^{-1}(a, b), [Ba] = 100 mmol L^{-1} and [Ti] = 100 mmol L^{-1} (c), and [Ba] = 50 mmol L^{-1} and [Ti] = 50 mmol L^{-1} (d), and heat treatment at 400 K, with corresponding particle sizes.

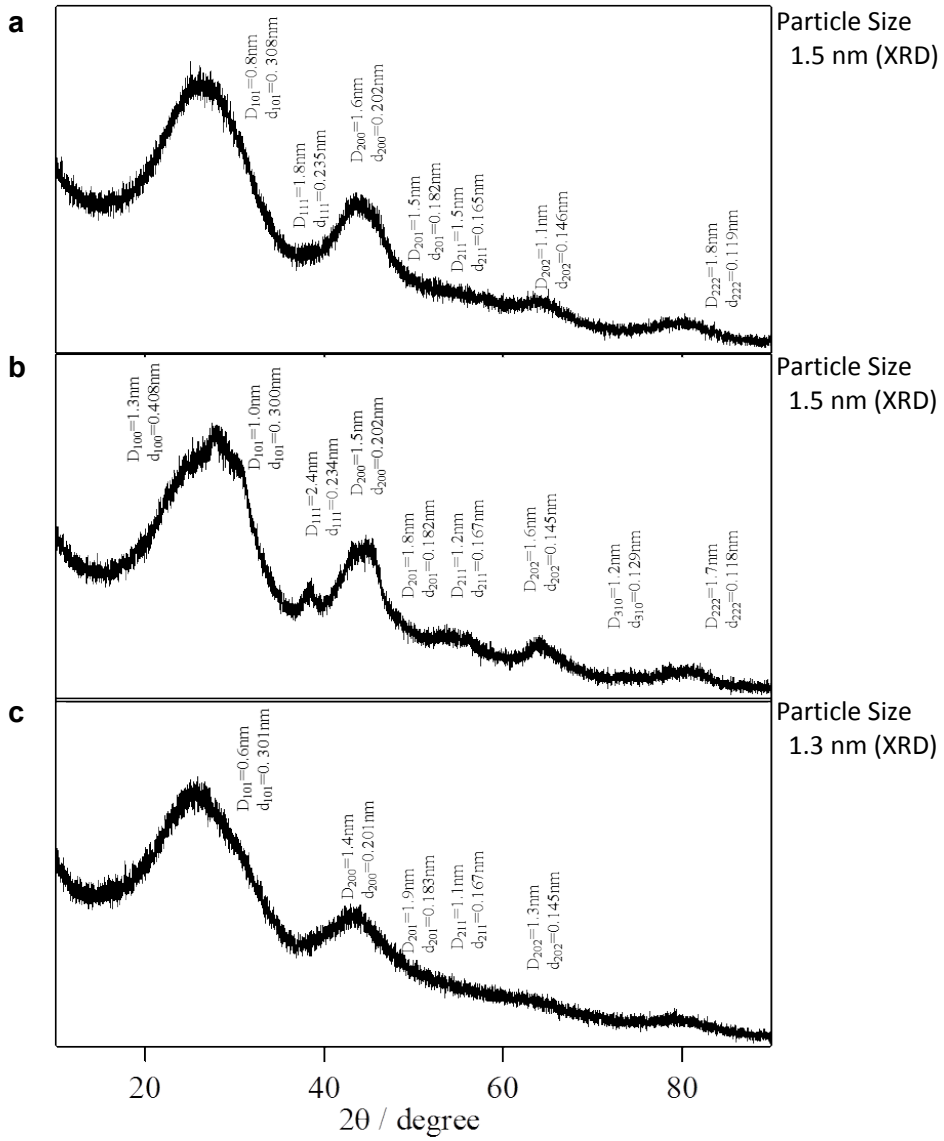

Figure S5-14. Evaluation of $BaTiO_3$ crystal structures. XRD patterns of confined-$BaTiO_3$ prepared under conditions [Ba] = 20 mmol L^{-1} and [Ti] = 10 mmol L^{-1}, and heat treatment at 400 K, with corresponding particle sizes.

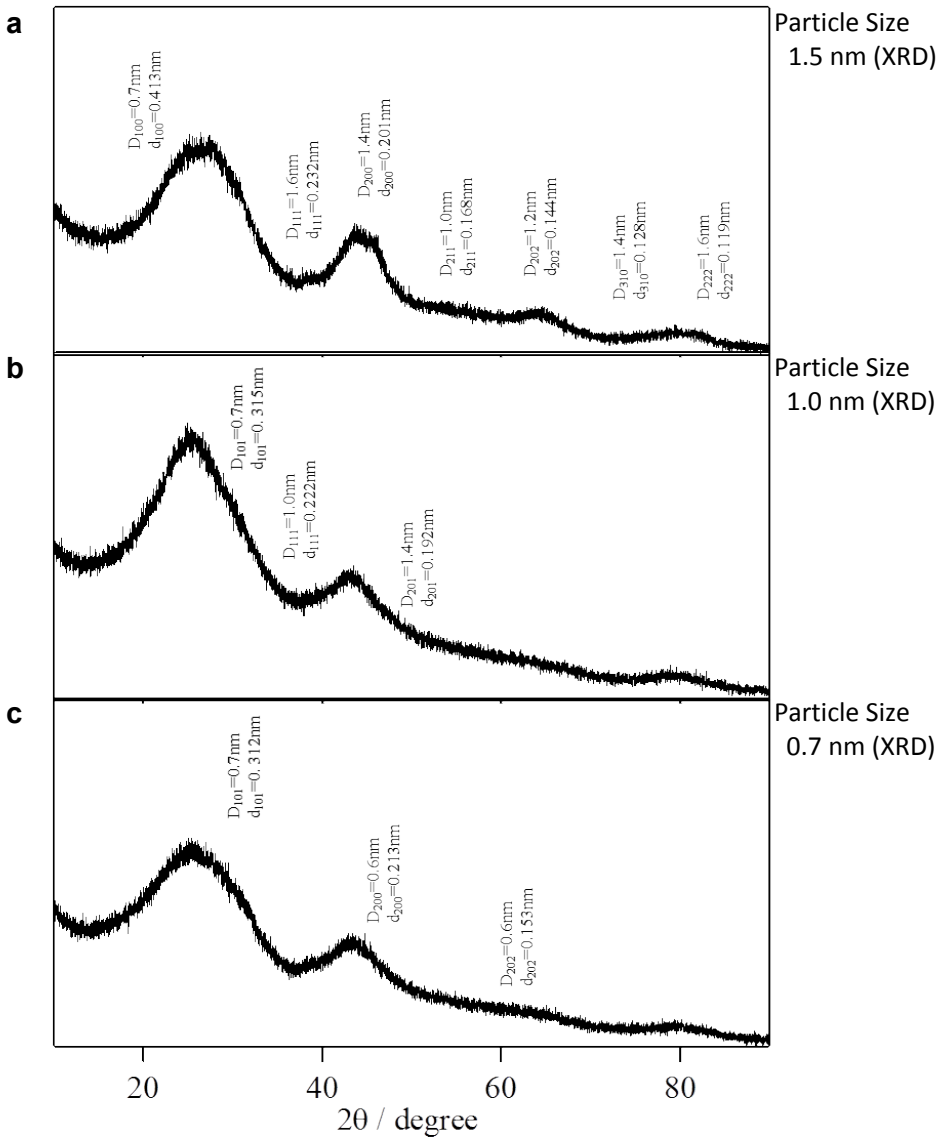

Figure S5-15. Evaluation of $BaTiO_3$ crystal structures. XRD patterns of confined-$BaTiO_3$ prepared under conditions [Ba] = 20 mmol L^{-1} and [Ti] = 10 mmol L^{-1}, and heat treatment at 400 K, with corresponding particle sizes.

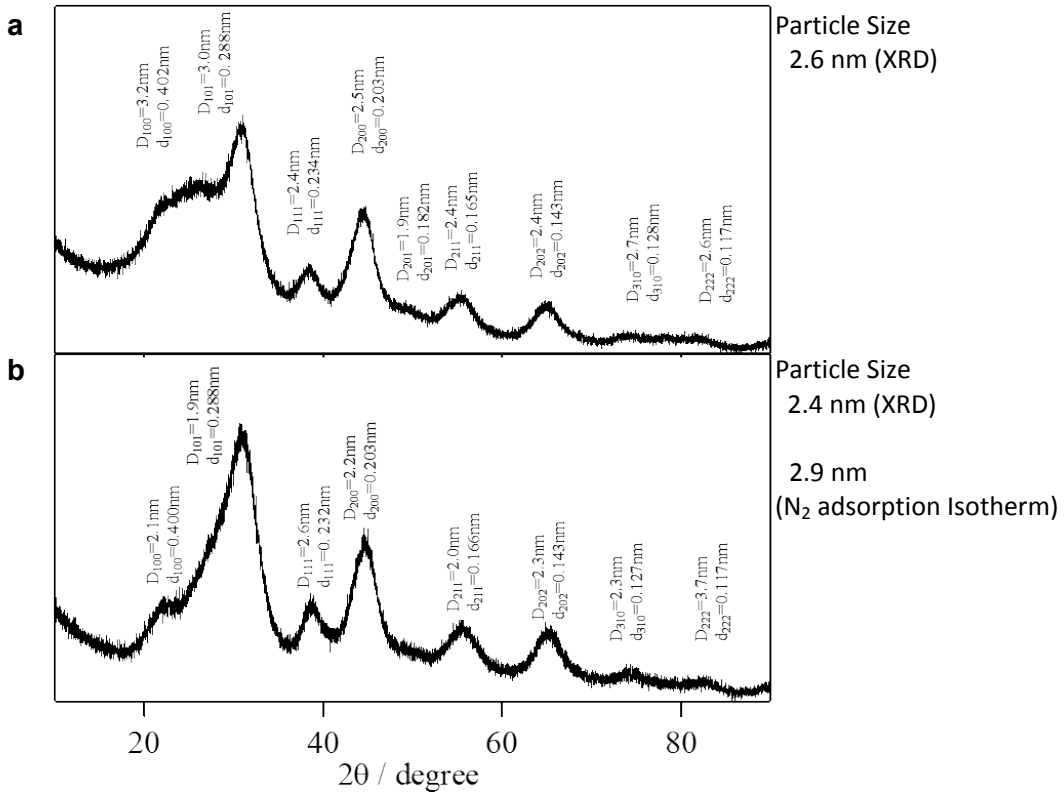

Figure S5-16. Evaluation of $BaTiO_3$ crystal structures. XRD patterns of confined-$BaTiO_3$ prepared under conditions [Ba] = 1200 mmol L^{-1} and [Ti] = 600 mmol L^{-1} (a) and after removal of ACFs (b), and heat treatment at 400 K, with corresponding particle sizes.

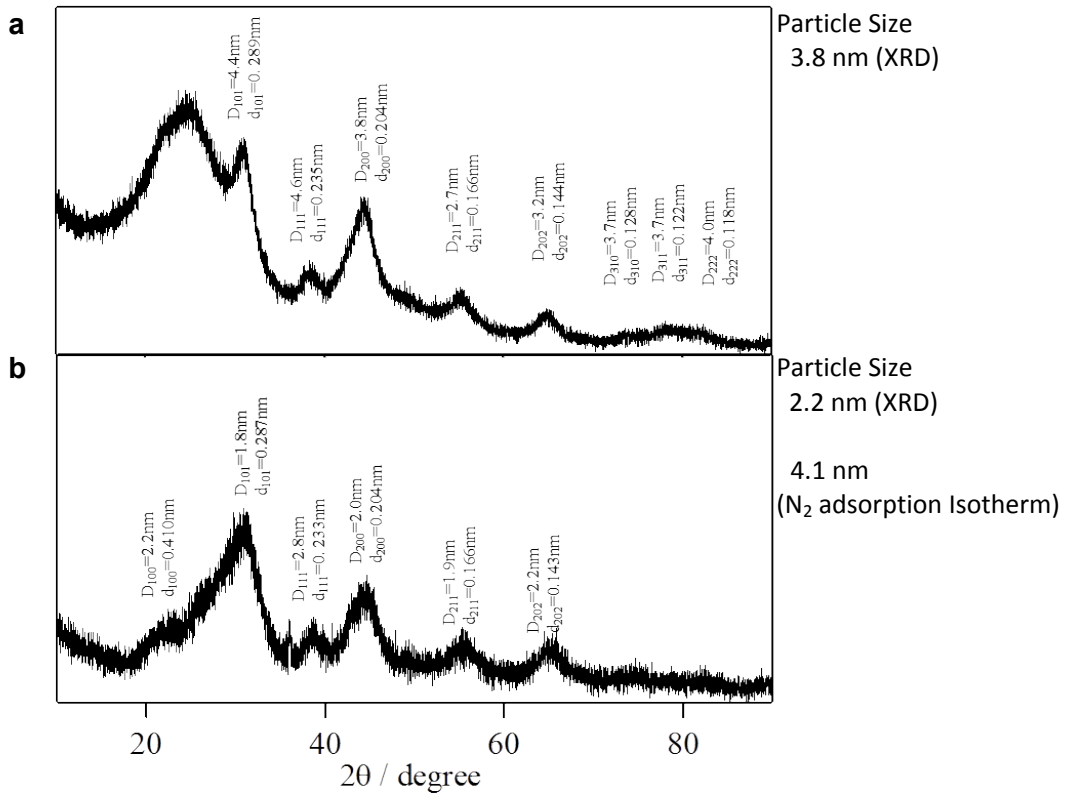

Figure S5-17. Evaluation of $BaTiO_3$ crystal structures. XRD patterns of confined-$BaTiO_3$ prepared under conditions [Ba] = 400 mmol L^{-1} and [Ti] = 200 mmol L^{-1} (a) and after removal of ACFs (b), and heat treatment at 400 K, with corresponding particle sizes.

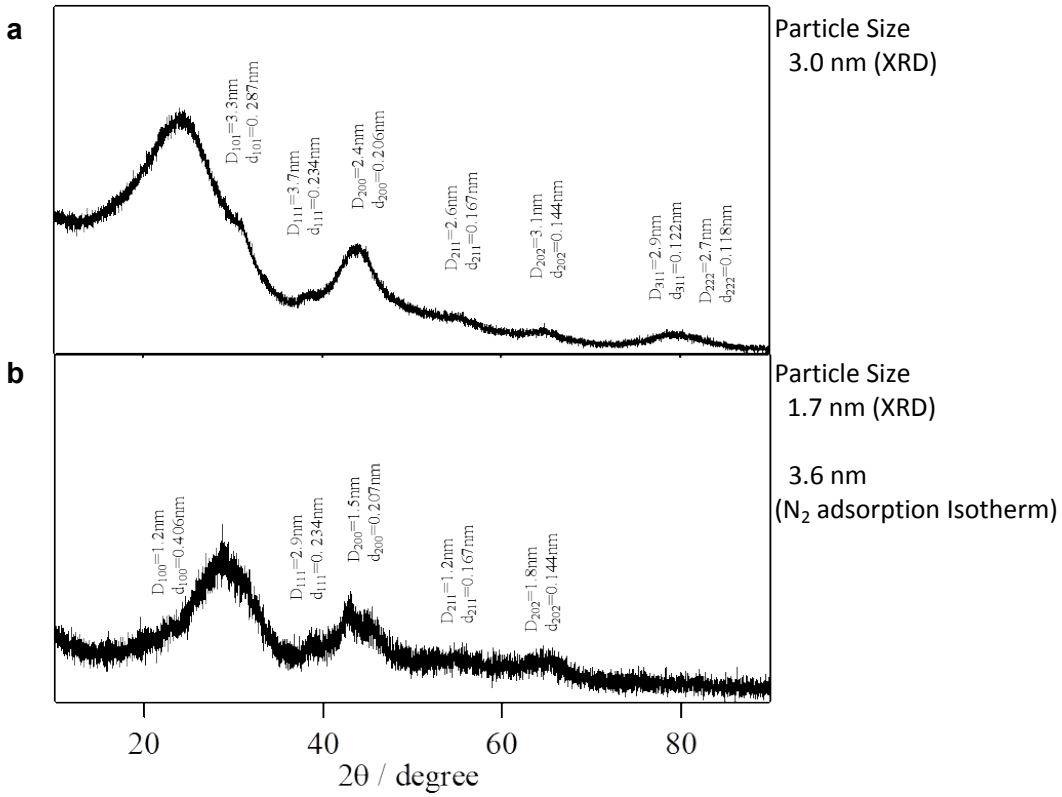

Figure S5-18. Evaluation of $BaTiO_3$ crystal structures. XRD patterns of confined-$BaTiO_3$ prepared under conditions [Ba] = 100 mmol L^{-1} and [Ti] = 50 mmol L^{-1} (a) and after removal of ACFs (b), and heat treatment at 400 K, with corresponding particle sizes.

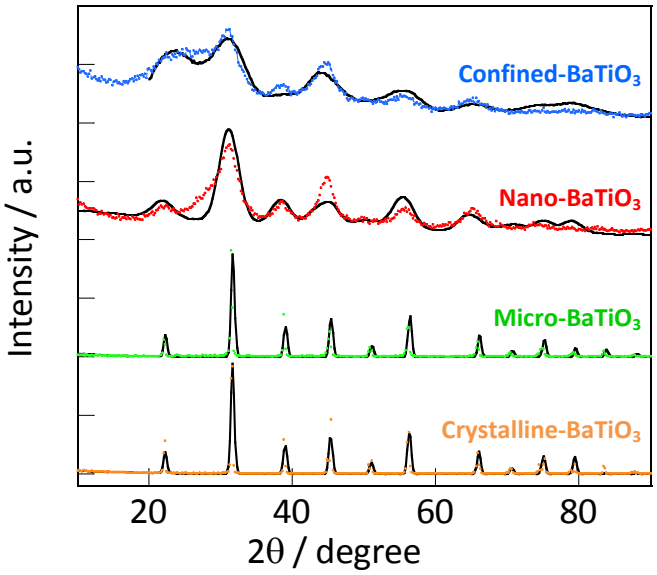

Figure S6. Evaluation of representative $BaTiO_3$ crystal structures. Experimental and simulated XRD patterns are indicated by coloured and black curves, respectively.